

# Irradiated ISM: Discriminating between Cosmic Rays and X-rays

R. Meijerink

*Sterrewacht Leiden, P.O. Box 9513, 2300 RA, Leiden, The Netherlands*

meijerin@strw.leidenuniv.nl

M. Spaans

*Kapteyn Astronomical Institute, P.O. Box 800, 9700 AV Groningen, The Netherlands*

spaans@astro.rug.nl

and

F.P. Israel

*Sterrewacht Leiden, P.O. Box 9513, 2300 RA, Leiden, The Netherlands*

israel@strw.leidenuniv.nl

## ABSTRACT

The ISM of active galaxy centers is exposed to a combination of cosmic ray, FUV and X-ray radiation. We apply PDR models to this ISM with both ‘normal’ and highly elevated ( $5 \times 10^{-15} \text{ s}^{-1}$ ) cosmic-ray rates and compare the results to those obtained for XDRs. Our existing PDR-XDR code is used to construct models over a  $10^3 - 10^5 \text{ cm}^{-3}$  density range and for  $0.16\text{-}160 \text{ erg s}^{-1} \text{ cm}^{-2}$  impinging fluxes. We obtain larger high  $J$  ( $J > 10$ ) CO ratios in PDRs when we use the highly elevated cosmic ray rate, but these are always exceeded by the corresponding XDR ratios. The [CI]  $609 \mu\text{m}/^{13}\text{CO}(2\text{-}1)$  line ratio is boosted by a factor of a few in PDRs with  $n \sim 10^3 \text{ cm}^{-3}$  exposed to a high cosmic ray rate. At higher densities ratios become identical irrespective of cosmic ray flux, while XDRs always show elevated [CI] emission per CO column. The HCN/CO and HCN/HCO<sup>+</sup> line ratios, combined with high  $J$  CO emission lines, are good diagnostics to distinguish between PDRs under either low or high cosmic ray irradiation conditions, and XDRs. Hence, the HIFI instrument on Herschel, which can detect these CO lines, will be crucial in the study of active galaxies.

*Subject headings:* ISM: X-rays — ISM: Cosmic Rays

## 1. Introduction

In centers of late-type galaxies, such as M 82, NGC 253, and Maffei 2, molecular line intensity ratios<sup>1</sup> are frequently found to be high, e.g.  $\text{CO}(4-3)/\text{CO}(1-0) \sim 60$  (Israel et al. 1995; White et al. 1994; Israel & Baas 2003) requiring high gas densities  $n > 10^{5.5} \text{ cm}^{-3}$ , and high temperatures of  $T \geq 50 \text{ K}$ . However, FUV photons are easily attenuated by dust and do not penetrate very deep into clouds and the galaxies are observed with beams covering regions typically hundreds of parsecs in size. At such large spatial scales, excited dense gas is not expected to have very large filling factors. UV radiation seems incapable of maintaining very large gas fractions at temperatures of  $T \sim 50 - 150 \text{ K}$ , and regular PDR models do not explain the observed high ratios. In addition, Israel & Baas (2002) have observed the [CI] 609  $\mu\text{m}$  line in the centers of late-type galaxies, and measured [CI] 609  $\mu\text{m}/^{13}\text{CO}(2-1)$  line intensity ratios in the range 20 – 60, which are hard to explain by (low-CR) PDR models. The  $\text{C}^+/\text{C}/\text{CO}$  transition zones in these PDRs contain only a thin layer in which neutral carbon has a high abundance. At the cloud edge, carbon is ionized, and deep in the cloud all carbon is locked up in CO.

Various authors have invoked elevated cosmic ray fluxes caused by greatly enhanced supernova rates in galaxy centers in order to explain large molecular gas masses at high temperatures (Suchkov et al. 1993; Bradford et al. 2003), and to explain high [CI] intensities and column densities relative to  $^{12}\text{CO}$  and  $^{13}\text{CO}$  (Pineau des Fôrets et al. 1992; Schilke et al. 1993; Flower et al. 1994). As most cosmic rays are produced in supernovae, their flux is proportional to the star formation rate, which is about  $1 \text{ M}_{\odot} \text{ yr}^{-1}$  for the Milky Way. In circumnuclear starbursts, star formation rates may be two orders of magnitude higher or more. Such galaxy centers may also contain an embedded accreting black hole producing X-rays. Like cosmic rays, but unlike UV photons, these X-rays can also penetrate through large column densities ( $N_H > 10^{24} \text{ cm}^{-2}$ ), and can cause the observed high line ratios over areas as large as 500 pc, when the emitted flux is high enough (Meijerink & Spaans 2005; Meijerink et al. 2006).

In this paper, we investigate whether in galaxy central regions PDRs with and without enhanced cosmic ray fluxes can be distinguished from XDRs on the basis of observable atomic and molecular line ratios. To this end, we calculate line intensities for PDRs with very different cosmic ray rates and compare the results to those obtained for XDRs with the same radiation fields and column densities.

---

<sup>1</sup>Intensity ratios of lines a to lines b are related to brightness temperature ratios by the cube of the line frequencies:  $(\nu_a/\nu_b)^3$

## 2. PDR and XDR models

We have constructed a set of PDR and XDR models from the codes described by Meijerink & Spaans (2005) and Meijerink et al. (2006), in which we varied both the incident radiation field and the density. The thermal balance (with line transfer) is calculated self-consistently with the chemical balance through iteration. Absorption cross sections for X-rays (1-100 keV) are smaller,  $\sim 1/E^3$ , than for FUV photons. Therefore, PDRs show a stratified structure while the changes in the chemical and thermal structure in XDRs are very gradual. Species like  $C^+$ , C and CO co-exist in XDRs, and large columns of neutral carbon (unlike in PDRs) are produced. In the XDRs, additional reactions for fast electrons that ionize, excite and heat the gas are included. The heating efficiency in XDRs is much higher. Since we focus on galaxy centers, we have assumed the metallicity to be twice Solar. We take the abundance of carbon to be equal to that of oxygen, since the carbon abundance increases faster than oxygen for larger metallicity. The precise C:O ratio does not affect our general results. We have calculated PDR models for both a ‘normal’ (low:  $\zeta = 5 \times 10^{-17} \text{ s}^{-1}$  – cf. van der Tak & van Dishoeck 2000) and a high ( $\zeta = 5 \times 10^{-15} \text{ s}^{-1}$ ) cosmic ray flux corresponding to a star formation rate of  $\sim 100 M_{\odot} \text{ yr}^{-1}$ . The model input parameters are summarized in Table 1. The range of free parameters ( $n = 10^3 - 10^5 \text{ cm}^{-3}$ ,  $G_0 = 10^2 - 10^5 / F_X = 0.16 - 160 \text{ erg s}^{-1} \text{ cm}^{-2}$ ) is representative for the conditions in galaxy centers. That is, from low- $J$  CO (critical density  $10^3 - 10^4 \text{ cm}^{-3}$ ) and HCN 1-0 (critical density  $\sim 10^5 \text{ cm}^{-3}$ ) observations it is apparent that gas in galaxy centers must exhibit the density range that we model. The irradiation conditions are typical for Milky Way PDRs like the Orion Bar (a high mass star-forming region) as well as a generic  $10^{44} \text{ erg s}^{-1}$  Seyfert nucleus X-ray luminosity for distances of about 100 pc and up.

## 3. Chemical and thermal structure

Higher cosmic ray (CR) ionization rates do not much affect the chemistry at the cloud edge, but large effects occur beyond the H/H<sub>2</sub> transition (see e.g. Fig. 1). As the CR flux in the PDRs is enhanced, electron, carbon and hydrogen abundances decrease much less beyond the H/H<sub>2</sub> transition, due to larger ionization/dissociation rates. Ion abundances also remain higher, causing H<sub>2</sub>O and OH to have higher abundances as well. As cosmic ray ionization contributes to the gas heating, higher incident CR fluxes raise gas temperatures deep in the cloud, with roughly  $T \sim \zeta^{1/3}$  at low densities ( $n \sim 10^3 \text{ cm}^{-3}$ ). At high densities,  $n = 10^5 \text{ cm}^{-3}$ , dust acts as an effective coolant if  $T > T_d$ , and the rise in the kinetic temperature is less pronounced. Both temperatures and abundances in a PDR become higher when CR rates are increased and ratios of emergent line emissions are also modified.

#### 4. CO line intensities and ratios

*a. Density  $n = 10^3 \text{ cm}^{-3}$*  (Table 2). In high-CR PDR clouds, a large fraction of all CO is dissociated, and CO is a factor  $\sim 100$  less abundant than in low-CR PDRs. However, in the latter, the CO lines are optically thick and CO line intensities are comparable for the same incident flux. In high-CR PDRs, the low- $J$  CO line ratios are somewhat larger than those in low-CR PDRs. The higher transitions show more of a difference and are diagnostically more valuable. In the XDRs, the CO gas temperature is on average much higher than in the PDRs, but marginally higher CO intensities occur only for the weak radiation field  $F_X = 1.6 \text{ ergs s}^{-1} \text{ cm}^{-2}$ . In XDRs with stronger radiation fields, CO line intensities are much lower than in PDRs, because column densities are too small to attenuate the X-rays significantly, and CO abundances are very low throughout the cloud. The very high CO(2-1)/CO(1-0) and CO(4-3)/CO(1-0) ratios in XDRs, which can be much higher than in the corresponding PDR cases, merely reflect the weakness of the lower  $J$  lines.

*b. Density  $n = 10^4 \text{ cm}^{-3}$*  (Table 3). High-CR PDRs have more intense CO lines than low-CR PDRs, but *their high- $J$ /low- $J$  CO line ratios* are only marginally higher than those of the corresponding low-CR PDRs. Again we find that XDR CO line intensities exceed those in PDRs in relatively weak radiation fields ( $G_0 = 10^3$  or  $F_X = 1.6 \text{ ergs s}^{-1} \text{ cm}^{-2}$ ). In XDRs with stronger radiation fields, the lower  $J$  CO lines (up to CO(4-3)) are much weaker than in PDRs, but the higher rotational lines are stronger. All XDR CO ratios are (much) larger than even the high-CR PDR CO ratios, and ratios at the intermediate and high  $J$  levels above CO(6-5) are diagnostically particularly meaningful.

*c. Density  $n = 10^5 \text{ cm}^{-3}$*  (Table 4). There are no longer significant differences between low-CR and high-CR PDRs. However, the XDR CO lines are strong in the lower transitions, and even more so at the intermediate and higher rotational transitions above CO(4-3). Their ratios are always larger than the corresponding ratios in any PDR model (see Meijerink et al. 2006 for a more detailed discussion). Some high- $J$  CO intensities and ratios are left blank, since no significant emission was found for these lines due to the low fractional abundances of CO and the high critical densities of the transitions.

#### 5. [CI] $609 \mu\text{m}/^{13}\text{CO}(2-1)$ ratios

XDRs, quite unlike PDRs, have significant neutral carbon abundances; their [CI] intensities behave as volume tracers. At the same time, XDRs generally have weaker low  $J$  CO and  $^{13}\text{CO}$  lines than PDRs, for  $n \leq 10^4 \text{ cm}^{-3}$  and  $F_X > 1 \text{ ergs s}^{-1} \text{ cm}^{-2}$ . Thus, in XDRs [CI]  $609 \mu\text{m}/^{13}\text{CO}(2-1)$  line intensity ratios are much larger than in corresponding PDRs.

Only at low densities,  $n \leq 10^3 \text{ cm}^{-3}$ , do high-CR PDRs behave in a fashion intermediate between XDRs and low-CR PDRs. In such low-density, high-CR PDRs, CO and  $^{13}\text{CO}$  dissociation causes simultaneous  $^{13}\text{CO}$  line weakening and [CI] line strengthening, resulting in [CI]/ $^{13}\text{CO}$  line intensity ratios four times higher than seen in low CR-PDRs, but still (much) lower than those seen in XDRs. Even at higher densities ( $n \geq 10^4 \text{ cm}^{-3}$ ) and stronger radiation fields ( $G_0 = 10^5$ ), the high-CR PDRs fail to produce [CI]/ $^{13}\text{CO}$  ratios more than 1.5 times those of low-CR PDRs. However, *in XDRs the [CI]/ $^{13}\text{CO}$  ratios remain very much larger* and thus provide an excellent tool to distinguish between PDRs and XDRs.

## 6. HCN/CO and HCN/HCO<sup>+</sup> ratios

Meijerink et al. (2006) found that HCN/CO and HCN/HCO<sup>+</sup> line intensity ratios distinguish between ‘normal’ (low-CR) PDRs and XDRs. These ratios are slightly different in high-CR PDRs. At densities of  $n = 10^4 \text{ cm}^{-3}$ , the HCN/CO ratios are lower in high-CR PDRs than in low-CR PDRs, especially for the  $J = 4 - 3$  transition, but they become more or less identical at densities of  $n = 10^5 \text{ cm}^{-3}$ . In XDRs, the HCN/CO ratios are almost invariably significantly lower than in either PDR. High-CR PDRs with densities of  $n = 10^4 \text{ cm}^{-3}$  have HCN/HCO<sup>+</sup> ratios *higher* than low-CR PDRs in the  $J = 1 - 0$  transition and *lower* than low-CR PDRs in the  $J = 4 - 3$  transition. This opposite behaviour reflects a cosmic ray induced shift in the HCN and HCO<sup>+</sup> abundances to larger (cooler) columns. However, at higher densities ( $n = 10^5 \text{ cm}^{-3}$ ), high-CR PDRs have HCN/HCO<sup>+</sup> ratios always lower than those in low-CR PDRs, mainly because of a boost in the HCO<sup>+</sup> production. In all cases where XDRs produce HCN and HCO<sup>+</sup> emission observable at all, the *HCN/HCO<sup>+</sup> ratios are (much) lower in the XDR than in either PDR.*

## 7. Conclusions

1. CO line intensity ratios increase when cosmic ray ionization rates are enhanced, but they remain smaller than those in XDRs. In particular high- $J$  ( $J > 10$ ) CO lines (which will become observable with HIFI in ESA’s Herschel space observatory) allow to distinguish between (high-CR) PDRs and XDRs. Using the HIFI time estimator and a beam filling factor of 0.05, we find that a line intensity of  $9 \times 10^{-6} \text{ erg s}^{-1} \text{ cm}^{-2}$ , the largest CO(16-15) intensity produced by our PDR models, will be detectable with HIFI in about 4 hours, while the very bright lines received from highly irradiated XDRs are detectable within minutes.
2. [CI] 609  $\mu\text{m}/^{13}\text{CO}(2-1)$  ratios are much higher in high-CR PDRs than in low-CR PDRs

at modest densities of  $n = 10^3 \text{ cm}^{-3}$ . At higher densities of  $n \geq 10^4 \text{ cm}^{-3}$ , this difference vanishes. In XDRs, the ratios are always larger than in PDRs at the same density, independent of incident radiation field.

3. HCN/CO and HCN/HCO<sup>+</sup> line ratios are good diagnostics to distinguish between PDRs and XDRs. As the ratios obtained for low-CR and high-CR PDRs are different, combination with high- $J$  CO lines is both crucial and profitable in the study of the active galaxy centers.
4. Although our model results broadly distinguish between low and high CR PDRs and XDRs, there is some degeneracy when constraining the four parameters (density, CR rate,  $G_0$  and  $F_X$ ) through individual ratios. Therefore, a combination of various ratios should be considered.

We thank J. le Bourlot and M. Elitzur for useful discussions on X-ray versus cosmic-ray irradiation, M. Hogerheijde and P. van der Werf for discussions on HIFI sensitivities, and an anonymous referee for his constructive comments.

## REFERENCES

- Bradford, C. M., Nikola, T., Stacey, G. J., Bolatto, A. D., Jackson, J. M., Savage, M. L., Davidson, J. A., & Higdon, S. J. 2003, ApJ, 586, 891
- Flower, D. R., Le Bourlot, J., Pineau des Fôrets, G., & Roueff, E. 1994, A&A, 282, 225
- Israel, F. P. & Baas, F. 2002, A&A, 383, 82
- . 2003, A&A, 404, 495
- Israel, F. P., White, G. J., & Baas, F. 1995, A&A, 302, 343
- Meijerink, R. & Spaans, M. 2005, A&A, 436, 397
- Meijerink, R., Spaans, M., & Israel, F. P. 2006, A&A, submitted
- Pineau des Fôrets, G., Roueff, E., & Flower, D. R. 1992, MNRAS, 258, 45P
- Schilke, P., Carlstrom, J. E., Keene, J., & Phillips, T. G. 1993, ApJ, 417, L67+
- Suchkov, A., Allen, R. J., & Heckman, T. M. 1993, ApJ, 413, 542

van der Tak, F. F. S. & van Dishoeck, E. F. 2000, *A&A*, 358, L79

White, G. J., Ellison, B., Claude, S., Dent, W. R. F., & Matheson, D. N. 1994, *A&A*, 284, L23

Table 1: PDR and XDR models

Density	PDR <sup>1</sup> ( $G_0$ )	XDR ( $F_x$ )	Size (pc)
$10^3$	$10^2, 10^3, 10^4$	0.16, 1.6, 16	10
$10^4$	$10^3, 10^4, 10^5$	1.6, 16, 160	1
$10^5$	$10^3, 10^4, 10^5$	1.6, 16, 160	1

<sup>1</sup> Both low and high CR PDRs are calculated.

Table 2: Line intensities ( $\text{erg s}^{-1} \text{ cm}^{-2} \text{ sr}^{-1}$ ) and ratios at density  $n = 10^3 \text{ cm}^{-3}$

Model Radiation field	Low-CR PDR			High-CR PDR			XDR		
	$G_0 = 10^2$	$G_0 = 10^3$	$G_0 = 10^4$	$G_0 = 10^2$	$G_0 = 10^3$	$G_0 = 10^4$	$F_x = 0.16$	$F_x = 1.6$	$F_x = 16$
CO(1-0)	8.2(-8)	8.6(-8)	1.0(-7)	8.4(-8)	8.3(-8)	8.1(-8)	1.2(-7)	3.7(-10)	3.0(-10)
CO(2-1)	4.8(-7)	5.1(-7)	6.6(-7)	6.3(-7)	6.3(-7)	6.4(-7)	1.0(-6)	9.3(-9)	9.1(-9)
CO(3-2)	9.4(-7)	9.9(-7)	1.5(-6)	1.6(-6)	1.6(-6)	1.6(-6)	2.8(-6)	3.4(-8)	5.2(-8)
CO(4-3)	1.4(-6)	1.6(-6)	2.8(-6)	2.2(-6)	2.1(-6)	2.1(-6)	4.5(-6)	5.3(-8)	1.1(-7)
CO(7-6)	3.2(-9)	1.1(-7)	7.8(-6)	1.4(-7)	1.2(-7)	1.3(-7)	-	3.4(-8)	1.1(-7)
CO(10-9)	8.4(-11)	1.7(-11)	2.3(-10)	9.2(-9)	4.7(-9)	2.4(-9)	-	-	-
CO(16-15)	-	1.0(-12)	1.2(-10)	-	4.2(-9)	7.1(-11)	-	-	-
$^{13}\text{CO}(2-1)$	2.1(-7)	2.1(-7)	2.8(-7)	1.1(-7)	1.0(-7)	9.7(-8)	8.1(-8)	1.8(-10)	1.6(-10)
[CI] 609 $\mu\text{m}$	5.6(-6)	7.2(-6)	8.9(-6)	1.1(-5)	1.2(-5)	1.4(-5)	3.6(-5)	1.0(-4)	1.2(-4)
CO(2-1)/CO(1-0)	5.9	5.9	6.3	7.5	7.6	7.8	8.4	25.4	30.3
CO(4-3)/CO(1-0)	17.0	18.7	27.2	26.2	25.6	25.8	36.2	1.5(2)	3.6(2)
CO(7-6)/CO(3-2)	3.4(-3)	1.1(-1)	5.2	8.6(-2)	7.9(-2)	8.0(-2)	-	9.8(-1)	2.2
CO(10-9)/CO(7-6)	2.5(-2)	1.5(-4)	3.0(-5)	6.7(-2)	3.7(-2)	1.9(-2)	-	-	-
CO(16-15)/CO(1-0)	-	1.2(-5)	1.1(-3)	-	5.0(-2)	8.7(-4)	-	-	-
CO(16-15)/CO(10-9)	-	6.2(-2)	0.51	-	9.0(-1)	3.0(-2)	-	-	-
[CI] 609 $\mu\text{m}/^{13}\text{CO}(2-1)$	26.7	34.1	31.5	97.1	1.2(2)	1.4(2)	4.4(2)	5.6(5)	7.4(5)

Table 3: Line intensities ( $\text{erg s}^{-1} \text{cm}^{-2} \text{sr}^{-1}$ ) and ratios at density  $n = 10^4 \text{cm}^{-3}$

Model Radiation field	Low-CR PDR			High-CR PDR			XDR		
	$G_0 = 10^3$	$G_0 = 10^4$	$G_0 = 10^5$	$G_0 = 10^3$	$G_0 = 10^4$	$G_0 = 10^5$	$F_x = 1.6$	$F_x = 16$	$F_x = 160$
CO(1-0)	1.6(-7)	1.9(-7)	2.5(-7)	2.1(-7)	2.4(-7)	2.7(-7)	2.6(-7)	1.4(-10)	3.4(-11)
CO(2-1)	1.2(-6)	1.6(-6)	2.0(-6)	1.8(-6)	2.0(-6)	2.4(-6)	3.5(-6)	5.2(-9)	1.4(-9)
CO(3-2)	3.4(-6)	4.6(-6)	6.2(-6)	5.3(-6)	6.2(-6)	7.5(-6)	1.3(-5)	4.0(-8)	1.0(-8)
CO(4-3)	5.7(-6)	8.5(-6)	1.2(-5)	1.0(-5)	1.2(-5)	1.5(-5)	2.9(-5)	1.7(-7)	4.3(-8)
CO(7-6)	2.9(-6)	1.3(-5)	2.7(-5)	1.6(-5)	2.3(-5)	3.5(-5)	9.7(-5)	1.8(-6)	6.4(-7)
CO(10-9)	2.4(-9)	7.4(-8)	1.8(-6)	2.4(-7)	1.0(-6)	4.9(-6)	1.1(-4)	3.5(-6)	1.6(-6)
CO(16-15)	1.1(-10)	6.8(-9)	2.3(-8)	2.1(-10)	3.1(-9)	2.9(-8)	1.1(-7)	2.5(-6)	1.7(-6)
HCN(1-0)	5.2(-9)	6.8(-9)	3.8(-9)	3.9(-9)	3.8(-9)	3.8(-9)	4.9(-10)	2.2(-13)	3.1(-14)
HCN(4-3)	3.3(-7)	4.0(-7)	1.0(-8)	9.5(-9)	1.0(-8)	1.0(-8)	1.3(-9)	4.0(-11)	3.2(-11)
HCO <sup>+</sup> (1-0)	1.9(-8)	2.2(-8)	2.6(-8)	1.1(-8)	1.1(-8)	1.1(-8)	1.5(-8)	1.0(-14)	1.4(-15)
HCO <sup>+</sup> (4-3)	4.3(-7)	6.6(-7)	7.9(-7)	6.2(-8)	7.0(-8)	7.2(-8)	2.0(-7)	1.0(-11)	1.4(-12)
<sup>13</sup> CO(2-1)	5.8(-7)	7.4(-7)	9.3(-7)	8.0(-7)	8.8(-7)	9.6(-7)	3.0(-7)	1.0(-10)	2.3(-11)
[Cl] 609 $\mu\text{m}$	8.4(-6)	9.9(-6)	1.1(-5)	1.2(-5)	1.4(-5)	1.7(-5)	5.2(-5)	1.2(-4)	1.2(-4)
CO(2-1)/CO(1-0)	7.8	8.1	8.2	8.4	8.6	8.8	13.3	36.9	39.6
CO(4-3)/CO(1-0)	35.8	44.2	50.4	47.5	51.8	56.9	1.1(2)	1.2(3)	1.3(3)
CO(7-6)/CO(3-2)	8.4(-1)	2.8	4.3	3.1	3.7	4.7	7.5	46.1	61.9
CO(10-9)/CO(7-6)	8.3(-4)	5.6(-3)	6.5(-2)	1.5(-2)	4.4(-2)	1.4(-1)	1.1	1.9	2.6
CO(16-15)/CO(1-0)	7.0(-4)	3.5(-2)	9.2(-2)	1.0(-3)	1.3(-2)	1.1(-1)	4.1(-1)	1.8(4)	5.0(4)
CO(16-15)/CO(10-9)	4.6(-2)	9.2(-2)	1.2(-2)	8.8(-4)	3.1(-3)	6.0(-3)	1.0(-3)	7.0(-1)	1.0
HCN(1-0)/CO(1-0)	3.2(-2)	3.5(-2)	3.4(-2)	1.9(-2)	1.6(-2)	1.4(-2)	1.9(-3)	1.6(-3)	9.1(-4)
HCN(4-3)/CO(4-3)	5.7(-2)	4.7(-2)	3.4(-2)	9.5(-4)	8.4(-4)	6.8(-4)	4.4(-5)	2.4(-4)	7.3(-4)
HCN(1-0)/HCO <sup>+</sup> (1-0)	2.8(-1)	3.1(-1)	3.3(-1)	3.6(-1)	3.4(-1)	3.6(-1)	3.2(-2)	21.7	22.6
HCN(4-3)/HCO <sup>+</sup> (4-3)	7.6(-1)	6.1(-1)	5.4(-1)	1.5(-1)	1.5(-1)	1.4(-1)	6.3(-3)	4.0	22.6
[Cl] 609 $\mu\text{m}/^{13}\text{CO}(2-1)$	14.6	13.4	12.1	14.9	16.2	17.6	1.7(2)	1.2(6)	5.1(6)

Table 4: Line intensities ( $\text{erg s}^{-1} \text{cm}^{-2} \text{sr}^{-1}$ ) and ratios at density  $n = 10^5 \text{cm}^{-3}$

Model Radiation field	Low-CR PDR			High-CR PDR			XDR		
	$G_0 = 10^3$	$G_0 = 10^4$	$G_0 = 10^5$	$G_0 = 10^3$	$G_0 = 10^4$	$G_0 = 10^5$	$F_x = 1.6$	$F_x = 16$	$F_x = 160$
CO(1-0)	3.1(-7)	4.1(-7)	5.5(-7)	3.3(-7)	4.3(-7)	5.6(-7)	7.6(-7)	1.4(-6)	1.2(-6)
CO(2-1)	2.7(-6)	3.5(-6)	4.7(-6)	2.8(-6)	3.7(-6)	4.9(-6)	7.1(-6)	1.4(-5)	1.5(-5)
CO(3-2)	8.5(-6)	1.2(-5)	1.6(-5)	9.1(-6)	1.2(-5)	1.7(-5)	2.5(-5)	5.2(-5)	6.2(-5)
CO(4-3)	1.8(-5)	2.5(-5)	3.6(-5)	1.9(-5)	2.7(-5)	3.7(-5)	5.6(-5)	1.2(-4)	1.7(-4)
CO(7-6)	3.6(-5)	8.0(-5)	1.4(-4)	4.4(-5)	8.8(-5)	1.4(-4)	2.1(-4)	6.6(-4)	1.0(-3)
CO(10-9)	4.3(-6)	7.7(-5)	2.4(-4)	1.2(-5)	9.0(-5)	2.7(-4)	3.7(-4)	1.6(-3)	2.9(-3)
CO(16-15)	2.1(-8)	7.8(-7)	5.1(-6)	2.2(-8)	7.9(-7)	8.8(-6)	5.1(-6)	4.3(-3)	8.6(-3)
HCN(1-0)	7.6(-8)	1.2(-7)	1.5(-7)	8.2(-8)	1.2(-7)	1.5(-7)	4.0(-8)	7.2(-8)	1.7(-8)
HCN(4-3)	2.5(-6)	3.2(-6)	3.7(-6)	2.6(-6)	3.2(-6)	3.7(-6)	1.4(-6)	2.2(-6)	7.0(-7)
HCO <sup>+</sup> (1-0)	5.8(-8)	8.4(-8)	1.1(-7)	9.6(-8)	1.5(-7)	2.3(-7)	1.6(-7)	5.2(-7)	1.7(-7)
HCO <sup>+</sup> (4-3)	1.8(-6)	2.9(-6)	4.0(-6)	3.3(-6)	5.0(-6)	6.8(-6)	4.2(-6)	8.9(-6)	9.8(-6)
<sup>13</sup> CO(2-1)	1.3(-6)	1.9(-6)	4.7(-6)	1.4(-6)	2.0(-6)	2.6(-6)	2.8(-6)	4.9(-6)	2.3(-6)
[Cl] 609 $\mu\text{m}$	7.4(-6)	8.7(-6)	9.8(-6)	9.1(-6)	1.1(-5)	1.3(-5)	4.1(-5)	1.1(-4)	4.4(-4)
CO(2-1)/CO(1-0)	8.6	8.5	8.5	8.6	8.6	8.7	9.3	10.0	12.2
CO(4-3)/CO(1-0)	56.6	61.1	64.6	57.8	62.3	66.2	73.1	91.1	1.3(2)
CO(7-6)/CO(3-2)	4.2	6.9	9.1	4.8	7.14	8.8	8.9	12.9	16.5
CO(10-9)/CO(7-6)	1.2(-1)	1.0	1.7	2.6(-1)	1.0	1.8	1.7	2.4	2.8
CO(16-15)/CO(1-0)	6.6(-2)	1.9	9.2	6.7(-2)	1.8	15.6	6.7	3.1(3)	6.9(3)
CO(16-15)/CO(10-9)	4.8(-3)	1.0(-2)	2.1(-2)	1.9(-3)	8.7(-3)	3.3(-2)	1.4(-2)	2.7	3.0
HCN(1-0)/CO(1-0)	2.4(-1)	2.8(-1)	2.8(-1)	2.5(-1)	2.7(-1)	2.7(-1)	5.2(-2)	5.1(-2)	1.3(-2)
HCN(4-3)/CO(4-3)	1.4(-1)	1.2(-1)	1.0(-1)	1.3(-1)	1.1(-1)	1.0(-1)	2.5(-2)	1.7(-2)	4.2(-3)
HCN(1-0)/HCO <sup>+</sup> (1-0)	1.3	1.4	1.4	8.5(-1)	8.0(-1)	6.7(-1)	2.5(-1)	1.4(-1)	9.9(-2)
HCN(4-3)/HCO <sup>+</sup> (4-3)	1.4	1.1	9.3(-1)	7.8(-1)	6.3(-1)	5.4(-1)	3.2(-1)	2.5(-1)	7.1(-2)
[Cl] 609 $\mu\text{m}$ / <sup>13</sup> CO(2-1)	5.7	4.5	3.6	6.3	5.5	4.8	14.7	24.0	1.9(2)

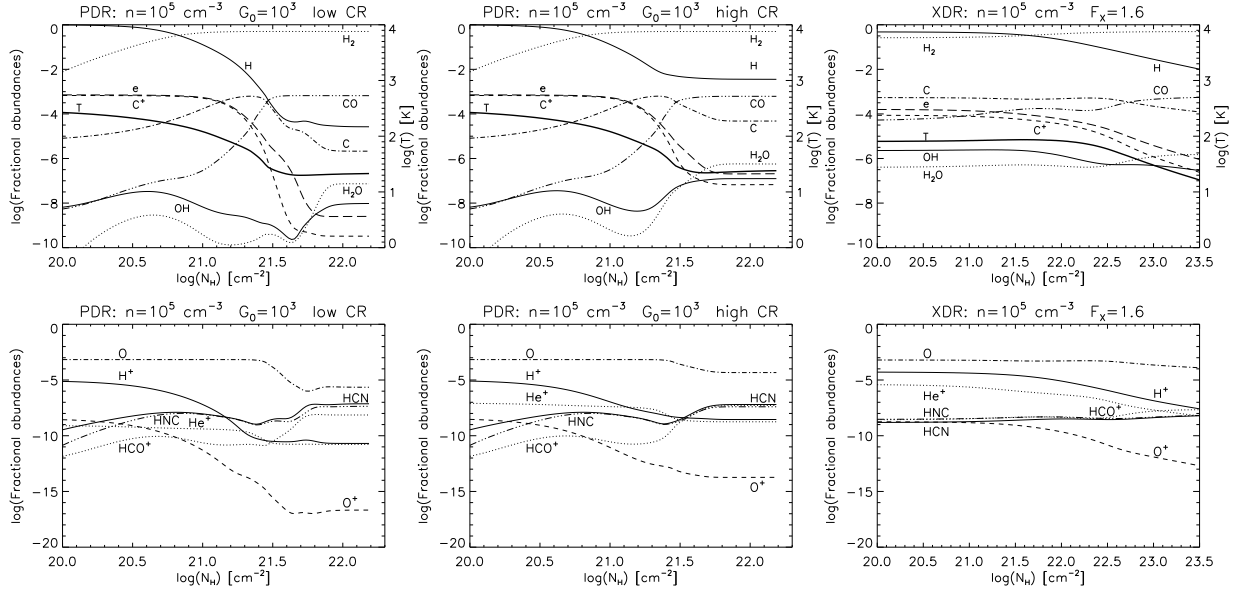


Fig. 1.— Chemical and thermal structure of PDR and XDR models at density  $n = 10^5 \text{ cm}^{-3}$  and  $G_0 = 10^3$  ( $F_X = 1.6 \text{ ergs s}^{-1} \text{ cm}^{-2}$ )